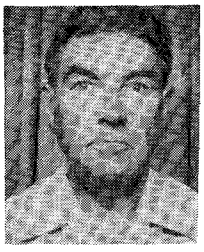

Clifford H. Champness was born in Surrey, England, in 1926. He received the B.Sc. in physics from the Imperial College of Science and Technology, in 1950, and was an exchange student in Eidgenossische Technische Hochschule, Zurich, in 1950–1951. He obtained the M.Sc. degree from the University of London, in 1957, and the Ph.D. degree from McGill University, Montreal, Quebec, Canada, in 1962.

From 1942–1947, he worked as an Assistant Experimental Officer on weapons development at the UK Ministry of Supply. As a Research Physicist at Associated Electrical Industries in Manchester, he investigated the transport properties of titanium dioxide, *III–V* compounds (mainly InAs and InSb), and treated the statistics of divalent impurity centers. From 1957–1960, he worked on silicon as a member of the Scientific Staff of the Research and Development Division of Northern Electric in Montreal. He was head of the Electronic Materials Department at the Noranda Research Centre, Pointe Claire, Quebec, from 1962–1967, where he directed work on thermoelectric cooling alloys based on bismuth telluride, epitaxial selenium film studies, and crystallization from amorphous selenium. In 1968, he was engaged as an Associate Professor by the Electrical Engineering Department of McGill University, where he has carried out research on the electronic and optical properties of selenium and tellurium. He was made full Professor in 1981. He has published over 50 papers on semiconductors, holds one patent, is a fellow of the former Physical Society of London, a member of the Canadian Association of Physicists, and a member of the American Physical Society.

An Analysis of an Electronically Tunable n-GaAs Distributed Oscillator

ASUO AISHIMA AND YOSHIFUMI FUKUSHIMA

Abstract—**The effective Schottky-barrier height of a contact to n-GaAs can be designed arbitrarily by interposing a thin, highly doped layer between a metal and n-GaAs and by controlling the thickness optimally. An n-GaAs diode with a Schottky-barrier cathode exhibits various space-charge modes depending on the barrier height. A traveling dipole domain mode in an n-GaAs diode changes into a cathode trapped domain mode as the injection current at the cathode decreases. It has been shown that an n-GaAs diode, which operates in a cathode trapped domain mode, exhibits a negative conductance over a fairly wide frequency range. A super wide-band electronically tunable distributed oscillator can be achieved by inserting an n-GaAs diode with a suitably designed Schottky-barrier cathode between resonant microstriplines in place of conventional dielectric material. It has been shown that the frequency of the distributed oscillator would be electronically tunable over a fairly wide frequency range from 9 to 26 GHz.**

NOMENCLATURE

$V(x)$	Potential in the diode.
q	Electronic charge.
ϵ	Permittivity.
N_L	Donor density in the active layer.
N_H	Donor density in the highly doped layer.
W	Length of the highly doped layer.
L	Length of the high-field layer in the active region.
V	Applied voltage.
Ψ	Wave function of electron.
m^*	Effective mass of the electrons in n-GaAs.
ζ	Eigenvalue of energy.
J_S	Current traversing from semiconductor to metal.
J_M	Current traversing from metal to semiconductor.
ϕ_{B0}	Work function in metal.
$\Delta\phi$	Barrier lowering due to image force.
T	Lattice temperature.
F_S	Fermi-Dirac distribution function in semiconductor.
F_M	Fermi-Dirac distribution function in metal.
E_d	Electric field at n^+–n interface.
$T(\eta)$	Transmission coefficient of electron.
ϕ_n	Potential difference between the Fermi level and the bottom of conduction band in GaAs.
A^*	Effective Richardson constant.
$n(x,t)$	Electron density.
$J(x,t)$	Conduction current density.
$E(x,t)$	Electric field.
$v(x,t)$	Electron velocity.
n_d	Donor density.
D_0	Diffusion constant of electron.
ω	Angular frequency.
$\tilde{n}(x,\omega)$	Small signal electron density.
$\tilde{J}(x,\omega)$	Small signal conduction current.
$\tilde{E}(x,\omega)$	Small signal electric field.
$\tilde{v}(x,\omega)$	Small signal electron velocity.
$\tilde{K}(x,\omega)$	Small signal total current.
$\tilde{\mu}(x,\omega)$	Differential mobility.
α, β, k	Propagation constant.
l	Length of the high-field layer in the active region.
l_1	Length of the low-field layer in the active region.

Manuscript received June 21, 1983; revised October 7, 1983.

The authors are with the Department of Electronics Engineering, Hiroshima University, Shitami, Saijohcho, Higashi-Hiroshima, 724 Japan.

0018-9480/84/0200-0157$01.00 ©1984 IEEE

$\tilde{Z}_h(\omega)$ Impedance of the high-field layer.
$\tilde{Z}_l(\omega)$ Impedance of the low-field layer.
n_0 Electron density in the high-field layer.
n_1 Electron density in the low-field layer.
σ_0 Conductivity in the low-field layer.
E_x Electric field traveling in the distributed oscillater along the line.
H_y Magnetic field traveling in the distributed oscillater along the line.
i_x Conduction current flowing across the line.
$\tilde{V}(z,\omega)$ Terminal voltage across the line.
$\tilde{Y}(\omega)$ Two terminal admittance.

I. Introduction

THE EFFECTIVE POTENTIAL barrier height of a Schottky contact to an n-GaAs can be controlled arbitrarily by interposing a thin, highly doped layer between a metal and the active layer of an n-GaAs [1], [2]. In order to control the barrier height, the thickness of the highly doped layer must be controlled precisely. Recent developments in molecular beam epitaxy and MOCVD make it possible to control the grown layer within an error of 50 Å. Therefore, the effective potential barrier height of a Schottky-barrier contact can be controlled to high precision by using such technologies.

It is well known that supercritically doped n-GaAs with ohmic electrodes at both ends exhibits Gunn oscillation [3]. When the usual ohmic contact at the cathode is replaced by a Schottky-barrier cathode, various space-charge modes of instabilities appear in the diode depending on the barrier height of the Schottky contact, which in turn depends on the thickness of the highly doped layer. One of the modes, named the cathode trapped domain mode by Aishima [5], does not exhibit large signal instabilities (traveling dipole domain mode) but another small signal instability (amplifier mode). Susceptance of the diode operating in the cathode trapped domain mode depends strongly on the length of the partially depleted layer, which in turn varies with applied voltage.

Yokoo *et al.* proposed theoretically after Watanabe *et al.* [9] an electronically tunable distributed oscillator and verified experimentally the performance of the device [6], [7]. The tunable range of the distributed oscillator was, however, only 2 GHz at *X*-band, since they constructed the distributed oscillator by using a subcritically doped n-GaAs diode. The susceptance change of this structure with voltage change is not so large as that of the supercritically doped diode with a Schottky cathode. One can expect a super wide-band electronically tunable distributed oscillator by using a supercritically doped diode in place of a subcritically doped diode, by replacing a usual ohmic cathode by a Schottky cathode, and by suitably controlling the thickness of the highly doped layer.

The purpose of the present paper is to propose a super wide-band electronically tunable distributed oscillator and to present some numerical results about the performance of the distributed oscillator.

II. Space-Charge Modes in an n-GaAs Diode with a Schottky-Barrier Cathode

It has already been reported that the effective Schottky-barrier height can be varied by interposing a thin, highly doped layer between a metal and the active layer of an n-GaAs diode and by suitably controlling the thickness of the highly doped layer. In this section, the injection current at the cathode and the space-charge modes in a metal, highly doped layer (n^+)–n-GaAs structure are calculated as a function of the thickness of the highly doped layer.

In Fig. 1 is shown a schematic energy diagram of a Schottky contact formed by a metal, highly doped layer (n^+)–n-GaAs structure. Here, we assume that the donor densities of the highly doped layer and the active n-type layer are N_H and N_L, respectively, and that the thickness of the highly doped layer and the high-field layer in the active region are W and L, respectively. We obtain the following equations for energy distribution by solving Poisson's equation:

$$V(x)=\frac{q}{2\epsilon}N_H x^2-\frac{q}{\epsilon}(N_L L+N_H W)x-\frac{q}{16\pi\epsilon x},\quad \text{for } 0<x<W \tag{1}$$

$$V(x)=\frac{q}{2\epsilon}N_L x^2-\frac{q}{\epsilon}N_L(W+L)x-\frac{q}{2\epsilon}(N_H-N_L)W^2-\frac{q}{16\pi\epsilon x},\quad \text{for } W\le x\le L \tag{2}$$

where

$$L=-W+\sqrt{\left(1-\frac{N_H}{N_L}\right)W^2+\frac{2\epsilon V}{qN_L}}\,. \tag{3}$$

The last terms in (1) and (2) are the energies due to the image force. Substituting (1) and (2) into Schroedinger's wave equation, we obtain

$$-\frac{\hbar^2}{2m^*}\nabla^2\psi+\left[\frac{q^2}{2\epsilon}N_H x^2-\frac{q^2}{\epsilon}(N_L L+N_H W)x-\frac{q^2}{16\Pi\epsilon x}\right]\cdot\psi=\zeta\psi,\quad \text{for } 0<x\le W \tag{4}$$

$$-\frac{\hbar^2}{2m^*}\nabla^2\psi+\left[\frac{q^2}{2\epsilon}N_L x^2-\frac{q^2}{\epsilon}N_L(L+W)x-\frac{q^2}{2\epsilon}(N_H-N_L)W^2-\frac{q^2}{16\Pi\epsilon x}\right]\psi=\zeta\psi,\quad \text{for } W<x\le L \tag{5}$$

where ζ is the eigenvalue of energy. The transmission coefficient and the reflection coefficient of electrons can be obtained by solving (4) and (5). It is, however, impossible to solve (4) and (5) analytically. Assuming that the potential varies slowly, the WKB approximation is applicable for calculating the transmission coefficient of electrons as follows:

$$T(\eta)=\left[\exp\left\{\frac{1}{\hbar}\int_{x_A}^{x_B}\sqrt{2m^*(V(x)-\zeta)}\,dx\right\}+\frac{1}{4}\exp\left\{-\frac{1}{\hbar}\int_{x_A}^{x_B}\sqrt{2m^*(V(x)-\zeta)}\,dx\right\}\right]^{-1}. \tag{6}$$

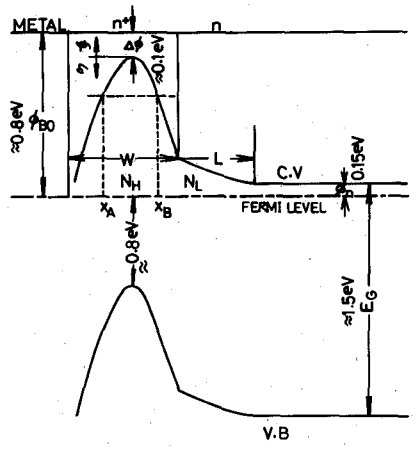

Fig. 1. Schematic potential energy diagram of Schottky contact formed by a metal n^+–n structure.

Electrons can traverse either from the semiconductor to the metal, or vice versa. The corresponding currents are designated as J_{SM} and J_{MS}, respectively. The observed current density is the algebraic sum of these two components [8]

$$J = J_{SM} - J_{MS}. \tag{8}$$

The current density equation for the first part, carriers traversing from the semiconductor to the metal, is

$$J_{SM} = \frac{A^*T}{k}\int_0^{\infty} \exp\left[-\frac{q(\phi_{B0} - \Delta\phi - \xi - V)}{kT}\right] d\xi + \frac{A^*T}{k}\int_0^{q(\phi_{B0}-\Delta\phi-\phi_n-V)} F_S(V)T(\eta)(1-F_M)\, d\eta. \tag{9}$$

For simplicity, the quantum-mechanical reflection coefficient of electrons with energy higher than the energy of the potential barrier maximum is assumed to be zero. The first term in the right-hand side of (9) is the thermionic component, and the second term is the tunneling component. F_S and F_M are the Fermi-Dirac distribution functions for the semiconductor and the metal, respectively

$$F_S = \frac{1}{1+\exp\left\{\dfrac{q(\phi_{B0} - \Delta\phi - \eta - V)}{kT}\right\}} \tag{10}$$

$$F_M = \frac{1}{1+\exp\left\{\dfrac{q(\phi_{B0} - \Delta\phi - \eta)}{kT}\right\}}. \tag{11}$$

The current equation for the second part, carrier traversing from the metal to the semiconductor, is

$$J_{MS} = \frac{A^*T}{k}\exp\left(\frac{-q\phi_{B0} + \Delta\phi}{kT}\right)\int_0^{\infty}\exp\left(-\frac{q\xi}{kT}\right) d\xi + \frac{A^*T}{k}\int_0^{q(\phi_{B0}-\Delta\phi-\phi_n-V)} F_M T(\eta)(1-F_S(V))\, d\eta. \tag{12}$$

Again, the first term is the thermionic component, and the second term is the tunneling component. Here, we define

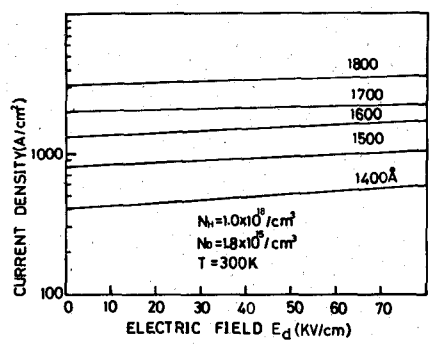

Fig. 2. Saturation current versus E_d for various thicknesses of the highly doped layer.

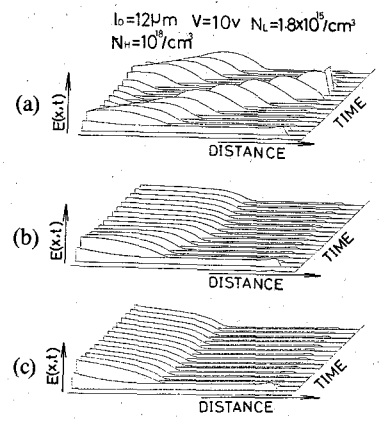

Fig. 3. Field distribution in the n-GaAs diode with a Schottky-barrier cathode. Traveling dipole domain mode changes into cathode trapped domain mode with decreasing thickness of the highly doped layer. (a) 1700 Å. (b) 1650 Å. (c) 1600 Å.

E_d as follows:

$$E_d = \frac{q}{\epsilon} N_L L. \tag{13}$$

E_d is the electric field at the n^+–n interface.

Fig. 2 shows the reverse saturation current versus E_d for various thicknesses of the highly doped layer, where N_H and N_L are assumed to be $1\times10^{18}/\text{cm}^3$ and $1.8\times10^{15}/\text{cm}^3$, respectively. As is seen in the figure, the reverse saturation current, namely, the effective barrier height, can be designed arbitrarily by suitably preparing the thickness of the highly doped layer.

The operation of the transferred electron device with such a Schottky-barrier cathode can be simulated by using the results obtained above.

Fig. 3 shows the field distribution in the diode, which is obtained numerically by solving Poisson's equation and equation of current continuity. In the calculations, an active region length of 12 μm, an applied voltage of 10, and a donor density of $1.8\times10^{15}/\text{cm}^3$ were assumed. As is clear in the figure, the traveling dipole domain mode changes into the cathode trapped domain mode as a thickness of the highly doped layer is decreased, that is, the supercritically doped diode is stabilized by suitably controlling the thickness of the highly doped layer. The stabilized diode, however, exhibits small signal instabilities over a wide frequency range.

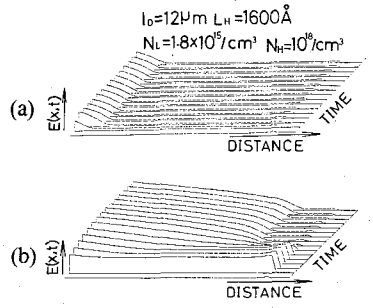

Fig. 4. Field distribution in the n-GaAs diode with Schottky-barrier cathode for applied voltages of 4 and 20. (a) $V = 4$ V. (b) $V = 20$ V.

Fig. 4 shows the intensity of field distribution versus distance for applied voltages of 4 and 20. The diode remains stabilized even at an applied voltage of 20.

III. Small Signal Impedance of Stabilized n-GaAs Diode

In this section, the small signal impedance of an n-GaAs diode with a Schottky-barrier cathode is calculated analytically. The analytical model is shown in Fig. 5. To avoid mathematical complications, the diode is divided into high and low constant field regions, as is seen in the figure. We followed the method of analysis given in [10]. The relevant equations for the analysis are as follows:

$$\frac{\partial n(x,t)}{\partial t} = -\frac{1}{q}\frac{\partial J(x,t)}{\partial t} \tag{14}$$

$$\frac{\partial E(x,t)}{\partial x} = \frac{q}{\epsilon}\{n(x,t) - n_d\} \tag{15}$$

$$J(x,t) = qn(x,t)v(x,t) - qD_0\frac{\partial n(x,t)}{\partial x}. \tag{16}$$

Physical quantities such as $n(x,t), v(x,t)$, etc., are described by adding spatially averaged dc terms to ac terms which vary spatially according to the terminal voltage change. It is convenient to restrict ourselves to the physical quantities which vary with time according to the complex exponential function $e^{j\omega t}$, where ω is the radian frequency. With the above-assumed time variation, all time derivatives may be replaced by $j\omega$. The linearized equations for small signal parameters can then be given by

$$j\omega\tilde{n}(x,\omega) = -\frac{1}{q}\frac{\partial \tilde{J}(x,\omega)}{\partial x} \tag{17}$$

$$\frac{\partial \tilde{E}(x,\omega)}{\partial x} = \frac{q}{\epsilon}\tilde{n}(x,\omega) \tag{18}$$

$$\tilde{J}(x,\omega) = qn_0\tilde{v}(x,\omega) + qv_0\tilde{n}(x,\omega) - qD_0\frac{\partial \tilde{n}(x,\omega)}{\partial x}. \tag{19}$$

Substituting (18) into the left-hand side of (17) and integrating

$$\tilde{J}(x,\omega) + j\omega\epsilon\tilde{E} = qn_0\tilde{v}(x,\omega) + qv_0\tilde{n}(x,\omega) - qD_0\frac{\partial \tilde{n}(x,\omega)}{\partial x} + j\omega\epsilon\tilde{E}(x,\omega) = \tilde{K}. \tag{20}$$

Substituting (18) into (20), and using the relation of $\tilde{v} = \tilde{\mu}\tilde{E}$,

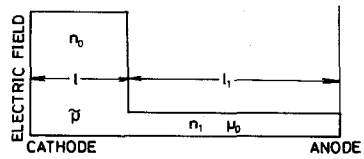

Fig. 5. A simplified diode model. The diode is divided into high- and low-field regions.

we obtain the differential equation for the electric field as follows:

$$\tilde{K} = -\epsilon D_0\frac{\partial^2\tilde{E}(x,\omega)}{\partial x^2} + \epsilon v_0\frac{\partial \tilde{E}(x,\omega)}{\partial x} + \{j\omega\epsilon + qn_0\tilde{\mu}\}\tilde{E}(x,\omega). \tag{21}$$

The solution of (22) can be expressed as

$$\tilde{E}(x,\omega) = Ae^{\alpha x} + Be^{\beta x} + \frac{\tilde{K}}{j\omega\epsilon + qn_0\tilde{\mu}} \tag{22}$$

where

$$\alpha = \frac{V_0 + \sqrt{V_0^2 + 4D_0\left(j\omega + \frac{qn_0\tilde{\mu}}{\epsilon}\right)}}{2D_0}$$

$$\beta = \frac{V_0 - \sqrt{V_0^2 + 4D_0\left(j\omega + \frac{qn_0\tilde{\mu}}{\epsilon}\right)}}{2D_0}. \tag{23}$$

The unknown coefficients A and B in (22) are uniquely determined from applying boundary conditions at both ends of the diode. The boundary condition at the Schottky cathode is

$$\tilde{K} = (\sigma_c + j\omega\epsilon)\tilde{E}(0,\omega) \tag{24}$$

where σ_c is the small signal injection conductance defined by

$$\sigma_c = \frac{\partial j}{\partial \tilde{E}(0,\omega)}. \tag{25}$$

The boundary condition at the anode was assumed to be ohmic. Substituting the determined values of A and B into (22), we obtain

$$\tilde{E}(x,\omega) = \frac{\tilde{K}}{(e^{\alpha l} - e^{\beta l})}\{e^{\beta l}(Z_b - Z_c) - Z_b\}e^{\alpha x} + \frac{\tilde{K}}{(e^{\alpha l} - e^{\beta l})}\{e^{\alpha l}(Z_c - Z_b) + Z_b\}e^{\beta x} + Z_b\tilde{K} \tag{26}$$

where

$$Z_c = \frac{l}{j\omega\epsilon + \sigma_c} \qquad Z_b = \frac{l}{j\omega\epsilon + qn_0\tilde{\mu}}. \tag{27}$$

The following impedance expression is easily obtained by integrating $\tilde{E}(x,\omega)$ over the diode length and dividing it by $\tilde{K}$:

$$\tilde{Z}_h(\omega) = \frac{(e^{\alpha l} - l)}{\alpha(e^{\alpha l} - e^{\beta l})}\{e^{\beta l}(Z_b - Z_c) - Z_b\} + \frac{(e^{\beta l} - l)}{\beta(e^{\alpha l} - e^{\beta l})}\{e^{\alpha l}(Z_c - Z_b) + Z_b\} + Z_b l. \tag{28}$$

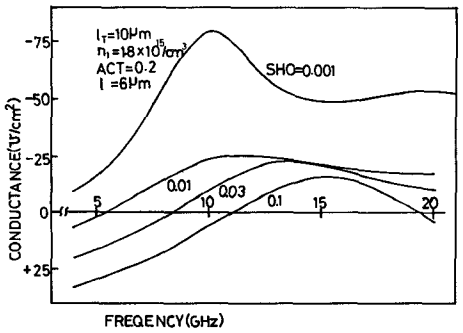

Fig. 6. Small signal negative conductance versus frequency for various injection characteristics at the cathode.

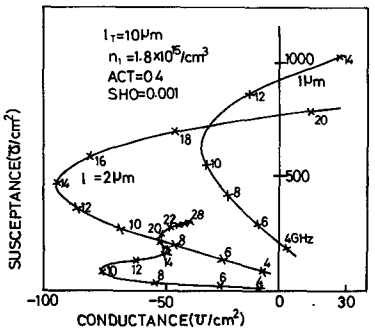

Fig. 7. Admittance chart for various thicknesses of the high-field layer. Susceptance reduces significantly with increasing length of the high-field layer.

The first and second term in the right-hand side of (28) are the impedances due to density modulation effects of carriers and the last term is the impedance due to velocity modulation effects.

In the low-field region, carrier confinement does not occur because of positive differential mobility, so the impedance is calculated approximately only by velocity modulation effects as follows:

$$\tilde{Z}_l(\omega) = \frac{l_1}{j\omega\epsilon + qn_1\mu_0}. \tag{29}$$

The diode terminal impedance is obtained by adding $\tilde{Z}_h(\omega)$ to $\tilde{Z}_l(\omega)$.

Fig. 6 shows the conductance calculated by the above-mentioned procedures versus frequency for various injection characteristics at the cathode, where SHO is the ratio σ_c to σ_0 and ACT is the ratio n_0 to n_1. In the calculation, a total diode length of 10 μm, a donor density of the low-field region of $1.8\times10^{15}/\text{cm}^3$, and a length of the high-field region of 6 μm were assumed. Density modulation effects of carriers, namely, space-charge transit time effects, reduce as a small signal injection current at the cathode decreases, so the impedance is mainly determined from the velocity modulation effects. This is the reason why the frequency range of negative conductance becomes wider as a small signal injection current decreases.

Fig. 7 shows admittance for various lengths of the high-field layer in the diode. The imaginary part of the admittance, namely, susceptance, reduces as a length of the highly doped layer increases. This characteristic can be used to construct a wide-band electronically tunable distributed oscillator.

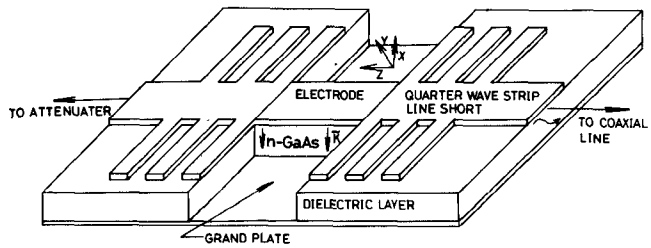

Fig. 8. Structure of distributed oscillator. An n-GaAs diode with a Schottky-barrier cathode is inserted into microstripline in place of conventional dielectric material.

IV. Propagation Constant of the Distributed

In this section, we calculate the propagation constant of a microstripline, into which an n-GaAs diode with the Schottky-barrier cathode, as analyzed in the preceding section, is inserted in place of the conventional dielectric.

As is seen in Fig. 8, the direction of a carrier drifting in the semiconductor is normal to the stripline, so that the Schottky electrode at the cathode and the ohmic electrode at the anode can be used as the conductors of the microstripline. Here, we assume that the electric field has an x component only, the wave propagates along the z-axis, and the electric field does not vary along the y-axis since the width of the microstripline is thin enough compared with the wavelength in the stripline.

Maxwell's wave equations reduce under these assumptions as follows:

$$\frac{\partial E_x}{\partial z} = -\mu\frac{\partial H_y}{\partial t} \tag{30}$$

$$\frac{\partial H_y}{\partial z} = -i_x - \epsilon\frac{\partial E_x}{\partial t} = -\tilde{K}. \tag{31}$$

Eliminating H_y from (30) and (31), we obtain

$$\frac{\partial^2 E_x}{\partial z^2} = \mu\frac{\partial \tilde{K}}{\partial t}. \tag{32}$$

Substituting $j\omega$ in place of $\partial/\partial t$ into (32) and integrating it over x, we obtain the following differential equation:

$$\frac{\partial^2 \tilde{V}(z,\omega)}{\partial z^2} - j\mu\omega\tilde{K}1 = 0 \tag{33}$$

where $\tilde{V}(z,\omega)$ is the voltage across the line and $\tilde{K}$ is the total current drifting in the n-GaAs. Substituting $\tilde{Y}(\omega)\tilde{V}(z,\omega)$ in place of $\tilde{K}$ into (33), we get

$$\frac{\partial^2 \tilde{V}(z,\omega)}{\partial z^2} - j\omega\mu 1\tilde{Y}(\omega)\tilde{V}(z,\omega) = 0 \tag{34}$$

where $\tilde{Y}(\omega)$ is the admittance of the n-GaAs analyzed in the preceding section. The solution of (34) can be expressed as

$$\tilde{V}(z,\omega) = C_1 e^{-kz} + C_2 e^{kz} \tag{35}$$

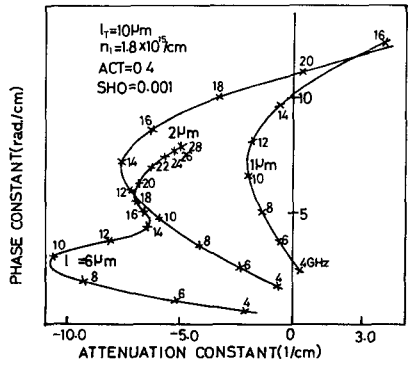

Fig. 9. Propagation constant calculated form the results shown in Fig. 7. A negative value of attenuation constant means that the wave grows with distance.

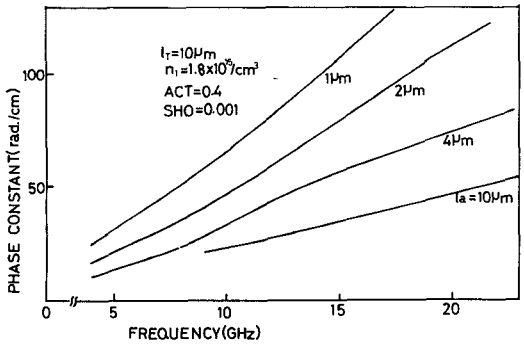

Fig. 10. Phase constant versus frequency for various thicknesses of the high-field layer. The phase constant is affected strongly by the thickness of the high-field layer.

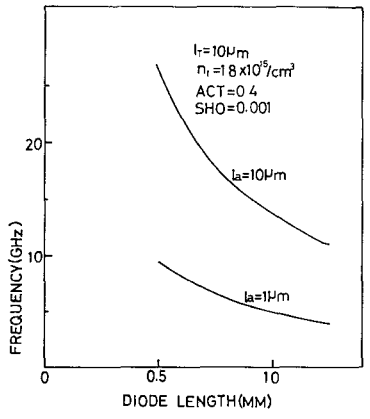

Fig. 11. Tuning range versus oscillator length along the stripline. The oscillator is tunable over a fairly wide frequency range from 9 GHz and 26 GHz for a oscillator length of 500 μm.

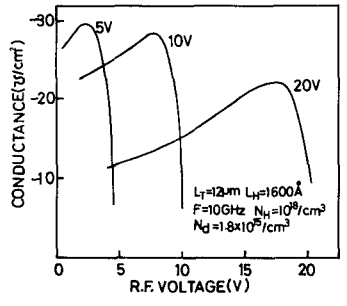

Fig. 12. Negative conductance versus ac voltage.

where the propagation constant k is given by

$$k = \sqrt{j\omega\mu 1 \tilde{Y}(\omega)}\,. \tag{36}$$

The real and the imaginary parts of k are the attenuation constant and the phase constant, respectively.

Fig. 9 shows the propagation constant of the microstripline calculated by using the results shown in Fig. 7, where a negative value of the attenuation constant means that the wave grows with distance. The phase constant reduces and the frequency range of wave growth broadens with increasing length of the high-field layer. As was pointed out previously [6], [7], one can construct a distributed oscillator, the frequency of which is determined from the phase constant and the length of the oscillator along the stripline, provided some fraction of the wave is reflected from either end of the diode along the line. To avoid mathematical complications, we assume that the cold loss of the line is zero and the reflective coefficient of both ends of the oscillator is unity. Then the oscillation conditions of the distributed oscillator are

$$\mathrm{Re}(k) < 0 \quad \mathrm{Im}(k)d = \pi \tag{37}$$

where d is the length of the oscillator along the line.

Fig. 10 shows the phase constant versus frequency for various lengths of the high-field layer, which is controlled by varying the terminal voltage. The phase constant is affected significantly by the high-field layer length. For example, the phase constant of the diode with a high-field layer length of 1 μm is 3.2 times greater than that of the diode with a high-field layer length of 10 μm at 10 GHz. This result means that one can realize super wide-band electronically tunable oscillators by using n-GaAs diodes with suitably controlled Schottky-barrier cathodes.

Fig. 11 shows the tuning range as a function of the diode length of the oscillator along the line. This figure summarizes the conclusive result of the present paper. As is seen in the figure, the tuning range of the oscillator varies as the length of the oscillator along the line changes. The tuning range of the oscillator is from 5 to 13 GHz for an oscillator with a length of 1 mm along the line. The oscillator is tunable over a wide frequency range from 9 to 26 GHz for an oscillator with a length of 500 μm along the line. This tuning range is ten times wider than that of a distributed oscillator utilizing a subcritically doped diode [6].

The analysis in Section III was carried out under small signal conditions. The method fails to estimate the output power of the oscillator. Hence, we performed a large signal computer simulation to calculate a diode terminal conductance as a function of ac voltage. The efficiency and output power can be determined from the results. The numerical method has been published elsewhere [11].

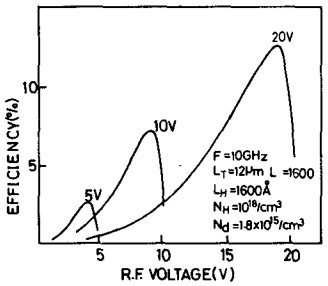

Fig. 13. Efficiency versus ac voltage. The high efficiency operation can be achieved for an oscillator with a suitably designed Schottky-barrier cathode.

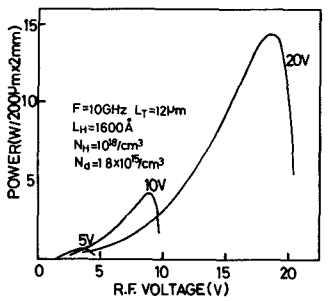

Fig. 14. Oscillation power versus ac voltage. The high oscillation power exceeding 10 W can be achieved in a single chip distributed oscillator.

Fig. 12 shows the negative conductance versus ac voltage for various applied voltages. At first, the negative conductance increases, then reaches a maximum value, and rapidly falls off as the ac voltage increases.

The efficiency is shown in Fig. 13 as a function of ac voltage. The maximum efficiency increases as the applied voltage increases. High efficiency, up to 13 percent, is attainable for an applied voltage of 20. As shown above, the efficiency for a diode with a suitably designed Schottky cathode exceeds the efficiency of the traveling dipole domain mode in a diode with an ohmic cathode. Such high-efficiency operation of a diode with a current limiting cathode was experimentally verified for an n − InP transferred electron device by Colliver *et al.* [12].

Fig. 14 shows the output power versus ac voltage for various applied voltages. The output power rapidly increases as an applied voltage increases. An output power of 15 W can be achieved for an oscillator with a width across the line of 200 μm and a length along the line of 2 mm. It should be noted, however, that the results shown in Fig. 14 give merely rough estimates of the oscillation power, since standing-wave phenomena in the oscillator considerably reduce the output power.

V. Conclusions

Numerical and analytical calculations have been made to investigate a super wide-band electronically tunable distributed oscillator. The following results have been obtained from the analysis.

Space-charge modes in a supercritically doped n-GaAs diode can be controlled by interposing a thin, highly doped layer between a metal and an n-GaAs layer and by suitably controlling the length of the highly doped layer. One of the modes, called the cathode trapped domain mode, exhibits negative conductance over a fairly wide frequency range because of the reduced space-charge transit time effects.

Inserting this diode between resonant microstriplines in place of the dielectric layer, a distributed oscillator can be realized. The phase constant of the distributed oscillator depends strongly on the thickness of the high-field layer in the diode, which in turn is controlled by the terminal voltage. The distributed oscillator is tunable over a wide frequency range from 9 to 26 GHz for an oscillator with a length of 500 μm along the line.

High efficiency, up to 13 percent, and high oscillation power exceeding 10 W are attainable for a distributed oscillator with a suitably designed Schottky-barrier cathode.

We have not considered the AM and FM noise in the oscillator. It is, however, well known that the amplitude of a negative resistance oscillator is relatively stable because of the nonlinearity of the negative resistance. FM noise is severely affected by the loaded quality factor of the circuit with the device susceptance included. The low quality factor of the external stripline resonator would worsen the FM noise behavior of the oscillator proposed in the present paper.

References

[1] T. Hariu and Y. Shibata, "Control of Schottky barrier height by thin high-doped layer," *Proc. IEEE*, vol. 63, pp. 1523–1524, Oct. 1975.

[2] C. N. Krishnan and R. Sharan, "Injection control in TED's by metal-n^+(thin)–n cathode structure," *IEEE Trans. Electron Devices*, vol. ED-24, pp. 1264–1265, Oct. 1977.

[3] D. E. MucCumber and A. G. Chynoweth, "Theory of negative-conductance amplification and of Gunn instabilities in "Two-Valley" semiconductors," *IEEE Trans. Electron Devices*, vol. ED-13, pp. 4–21, Jan. 1966.

[4] H. Kroemer, "Nonlinear space-charge domain dynamics in a semiconductor with negative differential mobility," *IEEE Trans. Electron Devices*, vol. ED-13, pp. 27–40, Jan. 1966.

[5] A. Aishima, A. Nishimura, and Y. Fukushima, "Various space charge modes in TED's with Schottky barrier cathode contact," *Japan J. Appl. Phys.*, vol. 18, pp. 1117–1125, June 1979.

[6] K. Yokoo, S. Ono, and Y. Shibata, "The electronic tunable Gunn diode oscillater," *Proc. IEEE*, vol. 57, pp. 494–496, May 1969.

[7] K. Yokoo and S. Ono, "Gunn diode distributed oscillater," *Trans. IECE of Japan* (in Japanese), vol. 58-B, p. 497, Oct. 1977.

[8] C. Y. Chang and S. M. Sze, "Carrier transport across metal-semiconductor barriers," *Solid-State Electron.*, vol. 13, pp. 727–740, 1970.

[9] N. Watanabe, J. Nishizawa, T. Yamamoto, and A. Shimizu, "Wide-band parametric amplifier utilizing distributed semiconductor diode," *Monograph of Technical Group of IECE Japan*, Jan. 1960 (in Japanese).

[10] J. Nishizawa and N. Watanabe, "High frequency power gain of the drift-type transistor," *The Science Reports of the Research Institutes of Tohoku University*, vol. 10(B), pp. 75–89, 1958.

[11] A. Aishima, K. Yokoo, and S. Ono, "An analysis of wide-band transferred electron devices," *IEEE Trans. Electron Devices*, vol. ED-25, pp. 640–645, June 1978.

[12] D. J. Colliver, K. W. Gray, and B. D. Joice, "High-efficiency microwave generation in InP," *Electron. Lett.*, vol. 8, pp. 11–12, Jan. 1972.

Asuo Aishima was born in Hiroshima Prefecture, Japan, in 1943. He received the B.S. and M.S. degrees in electrical engineering from Hiroshima University, Hiroshima, and the Ph.D. degree from Tohoku University, Sendai, Japan, in 1966, 1968, and 1979, respectively.

During the 1976–1977 academic year, he was on sabbatical leave at Tohoku University as a Visiting Research Fellow. He has been engaged in research work in the field of microwave semiconductor devices, high-field transport properties of semiconductor, and ballistic electron transport properties of *III–V* compounds.

Dr. Aishima is a member of the Institute of Electronics and Communication Engineers of Japan, and the Japan Society of Applied Physics.

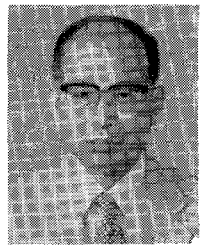

Yoshifumi Fukushima received the B.E., M.E., and Ph.D. degrees in electrical and communication engineering from Tohoku University, Sendai, Japan, in 1954, 1956, and 1960, respectively. His doctoral thesis focussed on the traveling-wave tube which had high power with wide band.

From 1961 to 1963, he was with the Electrical Communication Laboratory, Tohoku University, Sendai, as an Assistant Professor. From 1964 to 1967, he was Associate Professor in the Department of Electrical Engineering, Tohoku University, Sendai. Since 1968, he has been Professor at Hiroshima University, Hiroshima, Japan. His major studies include display devices, especially plasma display panels, secondary electron emission by ion bombardment, microwave semiconductor devices, and microwave theory.

Dr. Fukushima is a member of the Institute of Electronics and Communication Engineers of Japan (IECE), the Japan Society of Applied Physics (JSAP), and the Institute of Television Engineers of Japan (ITE).

Some Properties of the Matched, Symmetrical Six-Port Junction

GORDON P. RIBLET AND E. R. BERTIL HANSSON

Abstract—**Based on the *S*-matrix element-eigenvalue relations, the basic features of the matched, symmetrical, reciprocal six-port junction are derived. It is shown to be unsuitable for use in a six-port measurement system but can be used to build a five-way power divider. The equivalent admittance of the junction is derived, and, as an application, a stripline five-way power divider is designed. The theory is confirmed by the close agreement between computed and measured performance of an experimental one-to-five power divider.**

I. Introduction

ONE CLASS OF devices with, in general, *n*-fold axial symmetry are the symmetrical junctions. It is noteworthy that reciprocal junctions of this type up to and including the five-fold symmetrical junction were treated already in 1948 by Dicke [1]. Among the large number of other works on symmetrical junctions should be mentioned the book *Nonreciprocal Microwave Junctions and Circulators* by Helszajn [2]. However, as far as is known, the reciprocal, symmetrical six-port junction has never been given a detailed study in the literature.

Through the last few years, considerable interest has been focused on the six-port measurement technique, due largely to an important series of papers by Engen and Hoer [3]–[6]. The types of six-ports proposed so far have mostly been relatively complex, as in [6]. Attempts made to find simple types of suitable six-ports have resulted in narrowband devices [7], [8] with one exception, namely the symmetrical, reciprocal five-port junction combined with a directional coupler [9], [10]. One object of this paper is to examine the suitability of the symmetrical, reciprocal six-port junction for making six-port measurements.

Manuscript received April 4, 1983; revised September 6, 1983.

G. P. Riblet is with Microwave Development Laboratories, Inc., 11 Michigan Drive, Natick, MA 01760.

E. R. B. Hansson is with Kyber Product Consultants, Bjorke P. L. 8162, S-452 00 Strömstad Sweden.

II. Basic Properties of the Matched, Symmetrical, Reciprocal Six-Port Junction

A symmetrical six-port junction can be described by six complex quantities. Choosing initially for our description the scattering matrix, we have, at most, six different entries. By diagonalizing the scattering matrix, we get an alternative description of the junction in terms of the six eigenvalues of the scattering matrix. These eigenvalues constitute the reflection coefficients of the six possible eigenexcitations of the junction. The principle of conservation of energy requires that the scattering matrix eigenvalues be of unit amplitude for a lossless junction. A simple set of relations exists between the scattering matrix elements and its eigenvalues

$$S_{1I} = \frac{1}{6} \sum_{J=1}^{6} S_J e^{j(I-1)(J-1)(\pi/3)}, \qquad I = 1,2,\cdots,6 \quad (1)$$

where S_{1I} are the elements and S_I are the eigenvalues of the scattering matrix.

For a reciprocal, symmetrical six-port junction $S_{15} = S_{13}$ and $S_{16} = S_{12}$. From (1) it follows that $S_5 = S_3$ and $S_6 = S_2$.

0018-9480/84/0200-0164$01.00 ©1984 IEEE